2024 IEEE International Conference on Robotics and Automation (ICRA 2024)
May 13-17, 2024. Yokohama, Japan

The Joint-Space Reconstruction of Human Fingers by using a Highly Under-Actuated Exoskeleton

Yuan Su[1,2], Gaofeng Li[1], Yongsheng Deng[2], Ioannis Sarakoglou[3], Nikos G. Tsagarakis[3], and Jiming Chen[1]

***Abstract*— Hand motion tracking is essential in many fields, e.g., immersive virtual reality, teleoperation of robotic hand, and hand rehabilitation of stroke patient, as human hand plays a crucial role in our daily life. The highly under-actuated hand exoskeleton, which can track the 6-DoF motions of each fingertip via a highly under-actuated kinematic chain, exhibits many benefits in wearability and portability over other solutions. However, due to the non-anthropomorphic linkage, this hand exoskeleton also encounters difficulties in measuring human-finger's joint angles. While the joint-space is important in many scenarios, such as teleoperating a robotic hand with anthropomorphic kinematics but with different size to human. Here we proposed a new method to reconstruct the human finger joints by using a highly under-actuated hand exoskeleton. Our key contribution is the arc-fitting algorithm, which is able to calibrate the misalignment between the exoskeleton's and the human-finger's base frames and estimate the length of human's phalanxes, by using the fingertip's circular motions. With knowing the aforementioned informations, the joint angles can be reconstructed in high precision based on the inverse kinematics models of human fingers. Furthermore, our proposed method is compared with a baseline method, in which the joint angles obtained by a motion capture system are served as ground-truth. The results demonstrate that our proposed method exhibits excellent performance in reconstructing finger's joint configurations.**

***Index Terms*— Hand Motion Tracking, Hand Exoskeleton, Joint Reconstruction, Human-Robot Interaction**

I. Introduction

The dexterous hand, which is a primary effector organ of human beings, plays a crucial role in our daily life [1]. Thus, the hand motion tracking has significant values in many fields, such as immersive virtual reality, teleoperation of robotic hand, and hand rehabilitation of stroke patient.

In recent years, various methods have been proposed to achieve the motion tracking of human hands. Among them, visual-based methods are earliest. Visual-based hand tracking methods typically use stereo camera, e.g., Leap Motion [2], to capture hand images. Then human hand pose can be reconstructed via kinds methods. Some of these methods are implemented through training datasets, which are composed by RGB images [3]–[6]. Although these methods demonstrated good hand pose estimation performance, it is obviously that they do not meet the real-time requirements. To achieve online tracking, Handa *et. al.* [7] proposed a low-cost, vision-based teleoperation system, named by 'DexPilot', which can control a full 23-DOA robotic system by merely observing the human hand. Recently, an efficient hand gesture detection framework based on deep learning was proposed by Gao *et. al.* [8]. They designed a hand detection network for 3D hand detection and a hand classification network for gesture recognition, which were used in dexterous robot hand-arm teleoperation system. However, the accuracy and robustness of vision-based methods are generally unsatisfactory, since they are susceptible to external disturbances such as light changing and occlusion. In addition, the haptic feedback is missing in these methods.

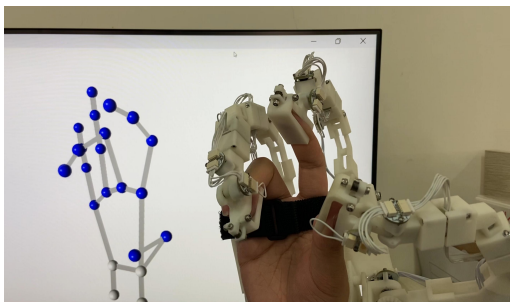

Fig. 1. The joint angles of human fingers is reconstructed in real-time by using a highly under-actuated hand exoskeleton.

To achieve high accuracy, kinds of wearable data gloves have been developed. Cyber-gloves [9] have been widely used due to their well performance in whole-hand motion tracking. However, the redundant use of single DOF sensors makes them bulky and requires complex algorithm to adapt to the difference of human palm sizes. To alleviate these issues, Glauser *et. al.* [10] proposed a stretch-sensing soft glove, which can interactively capture hand poses with high accuracy. Another group of data glove relies on inertial measurement units (IMUs) [11]. Baldi *et. al.* [12] proposed a sensing glove, called GESTO, which uses inertial and

This research is funded by the National Natural Science Foundation of China (NSFC) under Grant 62203426 and supported by NSFC under Grant 2088101.

[1]Y. Su, G. Li, and J. Chen are with the College of Control Science and Engineering, Zhejiang University, Hangzhou, 310027, China, and with the Key Laboratory of Collaborative Sensing and Autonomous Unmanned Systems of Zhejiang Province. (e-mails: yuansu@stumail.neu.edu.cn, gaofeng.li@zju.edu.cn, cjm@zju.edu.cn). Gaofeng Li is the corresponding author.

[2]Y. Su and Y. Deng are with the School of Mechanical Engineering and Automation, Northeastern University, Shenyang, 110819, China. (e-mails: yuansu@stumail.neu.edu.cn, yshdeng@mail.neu.edu.cn).

[3]I. Sarakoglou and N. G. Tsagarakis are with the Humanoids and Human Centered Mechatronics research line, Istituto Italiano Di Technologia, Via Morego 30, 16163, Genova, Italy. (e-mails: ioannis.sarakoglou@iit.it, nikos.tsagarakis@iit.it).

magnetic sensors for hand tracking. Santoni *et. al.* [13] presented a hand-tracking system based on magnetic positioning. It exhibited good performance with only a small number of electronics to be mounted on the hand. However a notable disadvantage of these gloves is their susceptibility to electromagnetic interference, which can deteriorate their performance. Recently, the fexible pressure sensors or electronic skins (e-skins) are attached to the back-palm to achieve motion tracking of human hands [14]. Although they show great advantages in lightweight and flexibility, the e-skins also suffer from an inherited shortage that the haptic feedback is absent.

Compared with the above solutions, the hand exoskeletons are getting rising attentions. Nycz *et. al.* [15] investigated a remote actuation system for wearable hand exoskeleton, which moves weight from the weakened limb to the shoulders. This design reduces the burden on the user and improving portability. Marconi *et. al.* [16] developed a hand exoskeleton with series elastic actuation, which can directly measure externally transferred torque and enable both position- and torque-controlled modes of operation. Owning to the ability in providing haptic feedback, hand exoskeletons are widely used in hand rehabilitations. However, they typically have a bulky structure and poor compatibility due to the high DoFs for better matching with the dexteriry of human hands.

To address the bulky problem of existing hand exoskeletons, a highly under-actuated hand exoskeleton was proposed in previous work [17], [18]. In this design, the linkages for each finger is composed of 5 passive and 1 active revolute joints. When the hand exoskeleton is installed on the back-palm, its linkages and the corresponding human's finger form a parallel mechanism with two parallel kinematic chains, in which the tips of the two chains are tethered. Thus the 6-DoF tracking of the fingertips is achieved through the forward kinematics of the mechanical chain. Although this mechanism is highly under-actuated, it can provide force feedback to both the extension and flexion of the fingers. In addition, owing to the highly under-actuated design, this exoskeleton exhibits great benefits in wearability and portability over other solutions.

However, one challenge arising with the highly under-actuated design is the difficulty in measuring the human-finger's joint angles. Due to non-anthropomorphic linkage, the hand exoskeleton eliminates the need for any alignment between the mechanical linkage and the operator's fingers. Thus the kinematic linkage can allow for unconstrained reach of the human fingers within their full workspace. But another negative result is that it is incapable of measuring human-finger's joint angles. While the joint-space is also important in many scenarios.

With knowing the fingertip's Cartesian poses, it seems to be straightforward to obtain the joint angles by using inverse kinematics of human fingers. However, the fingertip's poses are expressed in the exoskeleton's base frame instead of the human-finger's base frame. While the misalignment between the exoskeleton's and the human-finger's base frame is still unknown. In addition, length of fingers varies from person to person. These facts make the direct inverse kinematics infeasible.

To address the above issues, here we proposed a new method to reconstruct the joint-space configuration of human fingers by only using the fingertip's poses. As shown in Fig. 1, our main contributions are summarized:

- We presented an arc-fitting algorithm to calibrate the misalignment between the hand exoskeleton's and the human-finger's base frames and estimate the length of human's phalanxes.
- With knowing the aforementioned information, we reconstructed the joint angles in high precision based on the inverse kinematics models of human fingers.
- We design and conduct experiments to validate the effectiveness of the proposed method. The experimental results demonstrates excellent performance in reconstructing finger's joint configuration.

II. Problem Statement

In this paper, we would like to reconstruct the joint angles of a human finger by using a highly under-actuated hand exoskeleton, which can track the fingertip's 6-DoF motion with high resolution. Without loss of generality, we assume the human hand is a right hand. For the sake of convenience, the notations are defined in this section to formulate the problem.

In order to better describe the joint configuration of a human hand, the following frames are defined, as shown in Fig. 2.

- $\{W\}$: The world frame of the human hand, which is fixed on the hand exoskeleton above the back-palm.
- $\{B_i\}$: The base frame of each finger. Here $i = 1, 2, 3, 4, 5$ represents the thumb, the index, the middle, the ring, and the small finger, respectively.
- $\{EE_i\}$: The end-effector frames, which are fixed on the fingertips of each finger. The transformation of $\{EE_i\}$ relative to $\{W_i\}$ can be tracked by the hand exoskeleton in real-time.
- $\{L_{ij}\}$: The link frames, which are fixed on every phalanxes of each finger. Here $j = 1, 2, 3$ represents the proximal, the middle and the distal phalanx of each finger.

Based on the aforementioned definition, a finger can be modelled as a serial-link manipulator. To obtain the forward kinematic model of a finger, we make the following assumptions.

Assumption 1. *Each finger is composed of 4 revolute joints, in which the first and the second joint axes are perpendicular to each other.*

Assumption 2. *For each finger, its second, third and fourth joint axes are parallel to each other to implement the flexion and extension movements.*

Assumption 3. *For the index, the middle, the ring, and the small finger, their first joint axes are perpendicular to*

the palm to implement the lateral flexion movement, i.e., the orientation part of $\{B_i\}$ relative to $\{W\}$ is identity. For the thumb finger, as illustrated in Fig. 3, the direction of its first joint axis can be obtained by rotating the index/middle/ring/small finger's first joint axis around z_{B_i} by 45 degree and then rotating around x_{B_i} by -45 degree, successively. Here z_{B_i} and x_{B_i} represent the $z-$ and $x-$ axis of $\{B_i\}$ [19].

Then the transformation of $\{EE_i\}$ relative to $\{B_i\}$ can be calculated according to the forward kinematics:

$$^{B_i}T_{EE_i} = {}^{B_i}T_{L_{1i}} \cdot {}^{L_{1i}}T_{L_{2i}} \cdot {}^{L_{2i}}T_{L_{3i}} \cdot {}^{L_{3i}}T_{EE_i}, \quad (1)$$

where $^{B_i}T_{L_{1i}} = f(\theta_{1i}, \theta_{2i})$, $^{L_{1i}}T_{L_{2i}} = f(d_{1i}, \theta_{3i})$, $^{L_{2i}}T_{L_{3i}} = f(d_{2i}, \theta_{4i})$, $^{L_{3i}}T_{EE_i} = f(d_{3i})$, in which $\theta_{1i} \sim \theta_{4i}$ are the joint configurations of each finger and d_{1i}, d_{2i}, d_{3i} are the lengths of the proximal, the middle, and the distal phalanxes of each finger, respectively.

When the hand exoskeleton is installed on the back-palm, its linkages and the corresponding human's finger form a parallel mechanism with two parallel kinematic chains, in which the tips of the two chains are tethered. Therefore, it is possible to reconstruct the human hand's joint configuration by using the readings of the hand exoskeleton. For the convenience of the reconstruction, we also make the following assumptions according to human ergonomics:

Assumption 4. *For the joint angles, we have:*

$$\begin{aligned} &\textit{Thumb: } \theta_{11} \in \left[0, \frac{\pi}{3}\right], \theta_{j1} \in \left[0, \frac{\pi}{2}\right], \\ &\textit{Others: } \theta_{1i} \in \left[-\frac{\pi}{6}, \frac{\pi}{6}\right], \theta_{ji} \in \left[0, \frac{\pi}{2}\right]. \end{aligned} \quad (2)$$

When the finger is extended to the most, θ_{ji} = 0, i,j $\in [1, 5]$.

Assumption 5. *Although length of fingers varies from person to person, the ratios of each phalanxes are considered to be fixed for all human beings [20]. The ratios can be calculated according to the nominal values given in Table I.*

Upon the aforementioned assumptions, we can formulate our problem as follows:

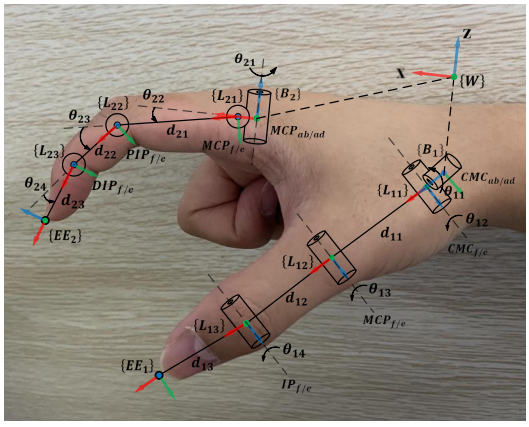

Fig. 2. The frames defined on the index and the thumb fingers. The frames attached on the middle, ring and small fingers are similar to the ones on the index finger.

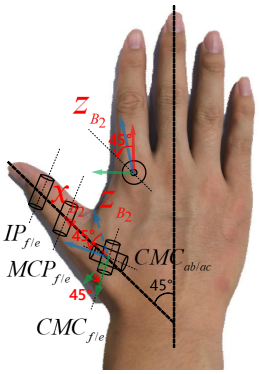

Fig. 3. Illustration of the first joint axis of the thumb.

TABLE I: The nominal lengths of all phalanxes for an adult.

	thumb	index	middle	ring	little
d_{1i}(m)	0.251	0.245	0.266	0.244	0.204
d_{2i}(m)	0.196	0.143	0.170	0.165	0.117
d_{3i}(m)	0.158	0.097	0.108	0.107	0.093

Problem 1. *Without knowing the translations from $\{W\}$ to $\{B_i\}$, and the lengths of each phalanx d_{ji}, we need to reconstruct the joint configurations θ_{ji} in real-time by given $^{W}T_{EE_i}$.*

III. Proposed Method

In order to reconstruct the joint angles of fingers, the transformation $^{B_i}T_{EE_i}$ needs to be captured. According to the kinematics tree, $^{B_i}T_{EE_i}$ can be calculated as follow:

$$^{B_i}T_{EE_i} = (^{W}T_{B_i})^{-1} \cdot {}^{W}T_{EE_i}, \quad (3)$$

where $^{W}T_{EE_i}$ can be tracked by the hand exoskeleton accurately, $^{W}T_{B_i}$ is the transformation of $\{B_i\}$ relative to $\{W\}$. Then the problem is transformed into solving $^{W}T_{B_i}$.

As stated in Section II, although different wears of the hand exoskeleton leads to different translations, the orientation of $\{B_i\}$ relative to $\{W\}$, i.e., $^{W}R_{B_i}$, can be considered as constant. Thus $^{W}R_{B_i}$ can be easily obtained according to **Assumption 3**. In this section, we will calibrate the translation from $\{W\}$ to $\{B_i\}$, estimate the lengths of all phalanxes d_{ji}, and finally reconstruct the joint angles of each finger.

A. Calibration of the Translation from $\{W\}$ to $\{B_i\}$

Let $P_i = [x_B^i, y_B^i, z_B^i]$ represents the position of $\{B_i\}$ relative to $\{W\}$. For each finger, the fingertip's trajectory is a circle if we only rotate the second joint while fixing the other joints, as shown in Fig. 4. Thus, P_i can be estimated through this circular motion.

In order to find proper P_i, the user would be asked to move only the second joint of the $i-$th finger and then the position trajectory of the fingertip can be recorded. Let χ_i denotes the collection of fingertip's position trajectory:

$$\chi_i = \{x_j^i, y_j^i, z_j^i | j = 1, 2, \cdots, N\}, \quad (4)$$

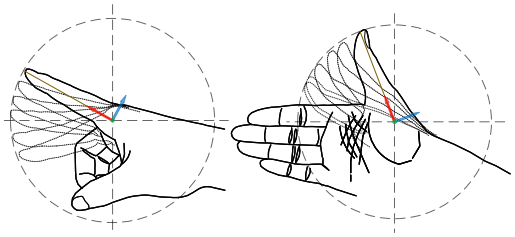

Fig. 4. The index and the thumb fingers moved as a circular arc around the base frame.

where x_j^i, y_j^i, z_j^i represents the position part of ${}^{W}T_{EE_i}$, N represents the data length of χ_i.

Then, all points in χ_i must satisfy the following function:

$$\left(x - x_B^i\right)^2 + \left(y - y_B^i\right)^2 + \left(z - z_B^i\right)^2 = L_{Total}^2, \tag{5}$$

where $L_{Total} = d_{1i} + d_{2i} + d_{3i}$ is the total length of all phalanxes of the $i-$th finger.

However, only Eq. (5) is not enough to locate P_i, because all points lies on the second joint axis can satisfy Eq. (5), since L_{Total} is unknown. To identify P_i, an extra constraint has to be considered, i.e., P_i and all points in χ_i are located in the same plane, denoted by $\mathcal{P}_c$. Therefore, our arc-fitting algorithm can be divided into two steps.

Step 1: Estimate the parameters of Plane $\mathcal{P}_c$

$\mathcal{P}_c$ can be formulated as:

$$z = a_0 x + a_1 y + a_2, \tag{6}$$

where a_0, a_1, a_2 are the parameters to describe the plane $\mathcal{P}_c$. Define the cost function as:

$$Q\left(a_0, a_1, a_2\right) = \sum_{j=1}^{N} \left(a_0 X_j + a_1 Y_j + a_2 - Z_j\right)^2, \tag{7}$$

where X_j, Y_j, Z_j represent the collection of x_j^i, y_j^i, z_j^i, respectively. We need to find the optimal estimation of a_0, a_1, a_2, denoted by $\hat{a}_0, \hat{a}_1, \hat{a}_2$, to minimize $Q\left(a_0, a_1, a_2\right)$. $\hat{a}_0, \hat{a}_1, \hat{a}_2$ can be obtained by using least-square method.

Step 2: Estimate P_i

Denote

$$\begin{aligned} a = -2x_B^i, b = -2y_B^i, c = -2z_B^i, \\ d = \left(x_B^i\right)^2 + \left(y_B^i\right)^2 + \left(z_B^i\right)^2 - L_{Total}^2, \end{aligned} \tag{8}$$

Then Eq. (5) is rewritten as:

$$x^2 + y^2 + z^2 + ax + by + cz + d = 0. \tag{9}$$

Then the error function can be defined as:

$$e_j = \sum_{j=1}^{N} X_j^2 + Y_j^2 + Z_j^2 + aX_j + bY_j + cZ_j + d. \tag{10}$$

Since $P_i \in \mathcal{P}_c$, then another constraint is introduced:

$$z_B^i = \hat{a}_0 x_B^i + \hat{a}_1 y_B^i + \hat{a}_2. \tag{11}$$

By replacing x_B^i, y_B^i, z_B^i with the parameters a, b, c (as shown in Eq. (8)), we can express the constraint as:

$$\hat{a}_0 a + \hat{a}_1 b - c - 2\hat{a}_2 = 0. \tag{12}$$

By using Langrange-Multiplier method, we can define the cost function as:

$$Q\left(a, b, c, d, \lambda\right) = \sum_{j=1}^{N} e_j^2 + \lambda\left(\hat{a}_0 a + \hat{a}_1 b - c - 2\hat{a}_2\right). \tag{13}$$

Then the least-square method can be employed to obtain the optimal estimation of $\hat{a}$, $\hat{b}$, $\hat{c}$, $\hat{d}$. Hence, according to Eq. (8), P_i is obtained by:

$$x_B^i = -\frac{1}{2}\hat{a},\ y_B^i = -\frac{1}{2}\hat{b},\ z_B^i = -\frac{1}{2}\hat{c} \tag{14}$$

B. Length Estimation of the Phalanxes

After knowing $\hat{a}$, $\hat{b}$, $\hat{c}$, $\hat{d}$, the total length L_{Total} can also be calculated according to Eq. (8):

$$L_{Total} = \sqrt{\left(x_B^i\right)^2 + \left(y_B^i\right)^2 + \left(z_B^i\right)^2 - \hat{d}}, \tag{15}$$

According to assumption 5, d_{1i}, d_{2i}, d_{3i} can be estimated by:

$$d_{ji} = L_{Total}\frac{\hat{d}_{ji}}{\hat{d}_{1i} + \hat{d}_{2i} + \hat{d}_{3i}}, \tag{16}$$

where $\hat{d}_{ji}$ is the nominal values given in Table I.

C. Calculation of Joint Angles via Inverse Kinematics

With the estimation results of P_i, ${}^{W}T_{B_i}$ can be established easily. Then ${}^{B_i}T_{EE_i}$ can be calculated in real time according to formula 3. Due to the kinematics model of the thumb and the other fingers established in Fig. 2 are similar, inverse kinematics solution of the thumb and the other fingers can be formulated in the same way. As shown in Fig. 5, joint configurations can be calculated as follow:

$$\theta_{1i} = atan(\frac{\varepsilon_i}{\epsilon_i}),\ \theta_{2i} = \beta_i - \gamma_i,\ \theta_{3i} = \pi - \varphi_i, \tag{17}$$

where,

$$\begin{aligned} \varepsilon_i = r_{24}, \epsilon_i = r_{14}, \beta_i = atan(\frac{\tau_i}{\alpha_i}), \\ \gamma_i = acos(\frac{{d_{1i}}^2 + {\delta_i}^2 - {d_{2i}}^2}{2d_{1i}\delta_i}), \\ \varphi_i = acos(\frac{d_{1i}^2 + {d_{2i}}^2 - {\delta_i}^2}{2d_{1i}d_{2i}}), \end{aligned} \tag{18}$$

where r_{ij} is the element of matrix ${}^{B_i}T_{EE_i}$ at the i-th row and the j-th column, $\tau_i = -r_{34} + d_{3i} \cdot r_{31}$, $\alpha_i =$

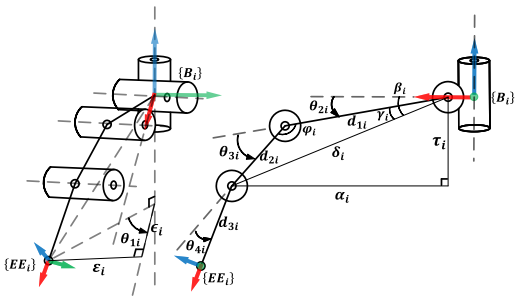

Fig. 5. General kinematic model for the thumb, the index, the middle, the ring and the little fingers.

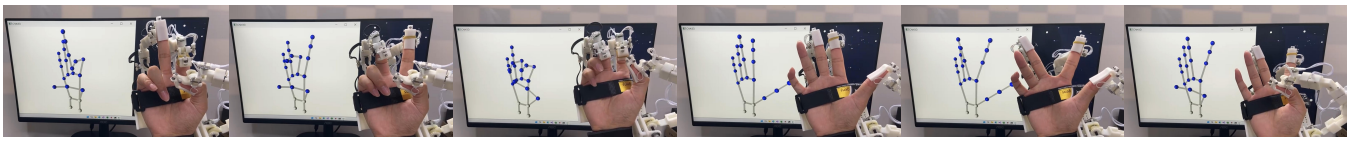

Fig. 6. Some snapshot of the real-time finger motion tracking process by using a highly under-actuated hand exoskeleton.

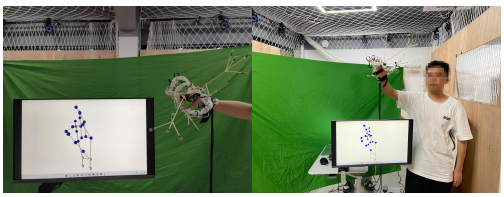

Fig. 7. Experimental Setups. Two frames which are measured by 4 optical markers are attached before and after a finger's joint, respectively, to measure the joint angles.

$\sqrt{{r_{14}}^2 + {r_{24}}^2} - d_{3i} \cdot r_{33}$. $\delta_i = \sqrt{{\tau_i}^2 + {\alpha_i}^2}$ is obtained by trigonometric relations. **Assumption 2** is used to dertermine the proper joint range.

Due to the coupling of finger joint configuration, the intra-finger constraints is used when solving θ_{4i}.

$$\theta_{4i} = \kappa\theta_{3i}, \tag{19}$$

where κ is a coefficient given in [19]. κ = 0.6, 0.32, 0.36, 0.16, 0.25 for the thumb, index, middle, ring and little finger, respectively.

IV. EXPERIMENTS

To validate the proposed method, a highly under-actuated hand exoskeleton was used which can track the position and orientation of the thumb, index and middle fingertips. It was an cost-effective one which designed under the reference of HEXOTRAC [18]. The tracked data ${}^{W}T_{EE_i}$ are transmitted to laptop for calculating the joint configuration via a UDP communication. The data is processed by a laptop (LENOVO IAH5R) with intel i5-12500H CPU.

A. Experimental Setups

In this work, the finger tracking ability of our method is demonstrated through a virtual anthropomorphic hand developed in CHAI3D. The virtual hand would accept the desired joint angles as inputs. The human finger's joint angle θ_{ji} is estimated by our proposed method then transfered into the CHAI3D at a frequency of 200Hz via a UDP communication. Some snapshots of the real-time finger motion tracking process is shown in Fig. 6.

To precisely evaluate the performance, the Opti-track system is used to obtain the ground-truths for comparison. As shown in fig. 7, two frames which are measured by 4 optical markers are attached before and after a finger's joint,respectively, to measure the joint angles.

Our method is compared with a baseline method, in which the translations from $\{W\}$ to $\{B_i\}$ are manually measured and the length of Phalanxes are the nominal values given in Table I. The detailed values of ${}^{W}T_{B_i}$ are given as:

$${}^{W}T_{B1} = \begin{bmatrix} 0.5 & 0.5 & 0.707 & 0 \\ -0.707 & 0.707 & 0 & 20 \\ 0.5 & 0.5 & 0.707 & -31 \\ 0 & 0 & 0 & 1 \end{bmatrix}, \tag{20}$$

$${}^{W}T_{B2} = \begin{bmatrix} I_3 & [70, 12, -17]^\top \\ [0,0,0] & 1 \end{bmatrix}, \tag{21}$$

$${}^{W}T_{B3} = \begin{bmatrix} I_3 & [70, -17, -17]^\top \\ [0,0,0] & 1 \end{bmatrix} \tag{22}$$

B. Results Analysis

Fig. 8 and Fig. 9 show the thumb joints tracking performance in a period of time and the deviation compared to Optitrack. As we can tell, our method exhibits good performance on tracking the CMC abduction/adduction joint, MCP flexion/extension joint and IP flexion/extension joint. However, there are still some issues in tracking the CMC flexion/extension joint. One possible reason for this phenomenon is the first and the second axes of the thumb are not orthogonal, which will become a direction for future breakthroughs.

Fig. 10 and Fig. 11 display the same experiment on the index finger. The tracking of MCP abduction/adduction joint is almost indistinguishable with the baseline method. Besides this, our Methods are all superior to the baseline method in tracking this finger. It is worth mentioning that the tracking of MCP flexion/extension joint is almost consistent with the ground-truth.

Fig. 12 and Fig. 13 shows the tracking performance of the middle finger. Our method also achieved good results compared to the baseline method.

V. CONCLUSION

In this paper, a simple but effective method was proposed to reconstruct the joint configuration of human fingers by using a highly under-actuated hand exoskeleton. The effectiveness of the proposed method was validated by experimental results.

There are still some issues remaining to be investigated in the future work. First, the kinematic model of the thumb still needs to be improved. In this paper, we assume that the first and the second axes of the thumb is orthogonal while they are not in fact. Second, it is worthy to investigate how to combine the joint-space information with the fingertips' Cartesian poses, in order to achieve better teleoperation performance for a robotic hand.

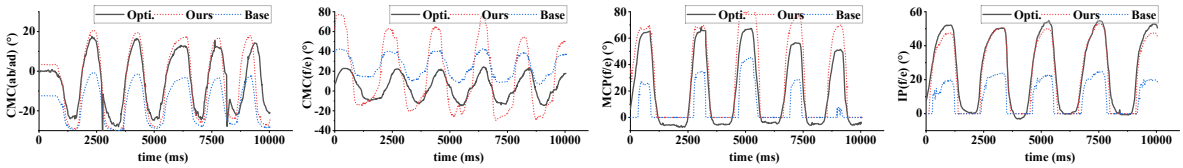

(a) (b) (c) (d)

Fig. 8. The thumb joints tracking performance. (a) CMC1. (b) CMC2. (c) MCP. (d) IP.

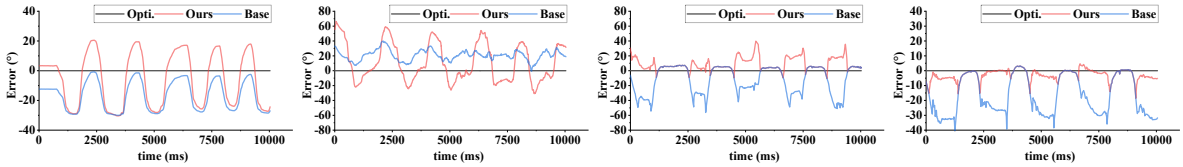

(a) (b) (c) (d)

Fig. 9. The thumb joints deviation compared to Optitrack. (a) CMC1. (b) CMC2. (c) MCP. (d) IP.

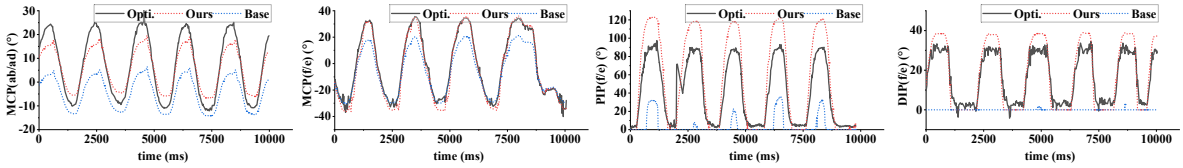

(a) (b) (c) (d)

Fig. 10. The index joints tracking performance. (a) MCP1. (b) MCP2. (c) PIP. (d) DIP.

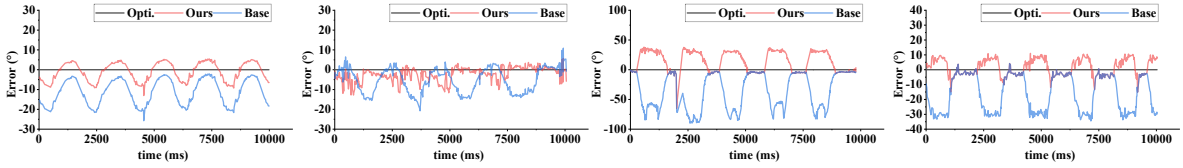

(a) (b) (c) (d)

Fig. 11. The index joints deviation compared to Optitrack. (a) MCP1. (b) MCP2. (c) PIP. (d) DIP.

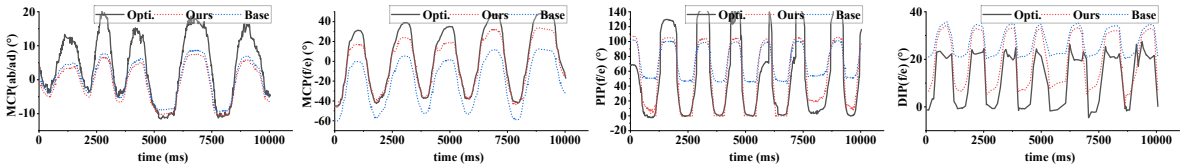

(a) (b) (c) (d)

Fig. 12. The middle joints tracking performance. (a) MCP1. (b) MCP2. (c) PIP. (d) DIP.

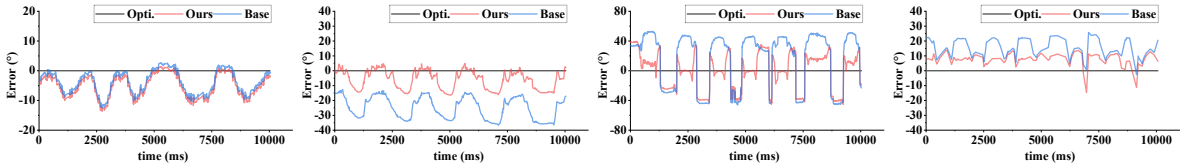

(a) (b) (c) (d)

Fig. 13. The middle joints deviation compared to Optitrack. (a) MCP1. (b) MCP2. (c) PIP. (d) DIP.

REFERENCES

[1] Y. Zhu, G. Wei, L. Ren, Z. Luo, and J. Shang. An anthropomorphic robotic finger with innate human-finger-like biomechanical advantages part ii: Flexible tendon sheath and grasping demonstration. *IEEE Transactions on Robotics*, 39(1):505–520, 2023.

[2] G. Marin, F. Dominio, and P. Zanuttigh. Hand gesture recognition with leap motion and kinect devices. In *2014 IEEE International Conference on Image Processing (ICIP)*, pages 1565–1569, 2014.

[3] L. Ge, Z. Ren, Y. Li, Z. Xue, Y. Wang, J. Cai, and J. Yuan. 3d hand shape and pose estimation from a single rgb image. In *Proceedings of the IEEE/CVF Conference on Computer Vision and Pattern Recognition (CVPR)*, June 2019.

[4] C. Zimmermann, D. Ceylan, J. Yang, B. Russell, M. Argus, and T. Brox. Freihand: A dataset for markerless capture of hand pose and shape from single rgb images. In *Proceedings of the IEEE/CVF International Conference on Computer Vision (ICCV)*, October 2019.

[5] Z. Zhang, S. Xie, M. Chen, and H. Zhu. Handaugment: A simple data augmentation method for depth-based 3d hand pose estimation. In *Proceedings of the IEEE/CVF Conference on Computer Vision and Pattern Recognition (CVPR)*, 2020.

[6] S. Hampali, M. Rad, M. Oberweger, and V. Lepetit. Honnotate: A method for 3d annotation of hand and object poses. In *Proceedings of the IEEE/CVF Conference on Computer Vision and Pattern Recognition (CVPR)*, 2020.

[7] A. Handa, K.V. Wyk, W. Yang, J. Liang, Y.W. Chao, Q. Wan, S. Birchfield, N. Ratliff, and D. Fox. Dexpilot: Vision-based teleoperation of dexterous robotic hand-arm system. In *2020 IEEE International Conference on Robotics and Automation (ICRA)*, pages 9164–9170, 2020.

[8] Q. Gao, Z. Ju, Y. Chen, Q. Wang, and C. Chi. An efficient rgb-d hand gesture detection framework for dexterous robot hand-arm teleoperation system. *IEEE Transactions on Human-Machine Systems*, 53(1):13–23, 2023.

[9] L. Almeida, E. Lopes, B. Yalçinkaya, R. Martins, A. Lopes, P. Menezes, and G. Pires. Towards natural interaction in immersive reality with a cyber-glove. In *2019 IEEE International Conference on Systems, Man and Cybernetics (SMC)*, pages 2653–2658, 2019.

[10] O. Glauser, S. Wu, D. Panozzo, O. Hilliges, and O. Sorkine-Hornung. Interactive hand pose estimation using a stretch-sensing soft glove. *Association for Computing Machinery*, 38(4), jul 2019.

[11] T.L. Baldi, M. Mohammadi, S. Scheggi, and D. Prattichizzo. Using inertial and magnetic sensors for hand tracking and rendering in wearable haptics. In *2015 IEEE World Haptics Conference (WHC)*, pages 381–387, 2015.

[12] T. L. Baldi, S. Scheggi, L. Meli, M. Mohammadi, and D. Prattichizzo. Gesto: A glove for enhanced sensing and touching based on inertial and magnetic sensors for hand tracking and cutaneous feedback. *IEEE Transactions on Human-Machine Systems*, 47(6):1066–1076, 2017.

[13] F. Santoni, A.D. Angelis, A. Moschitta, and P. Carbone. Magik: A hand-tracking magnetic positioning system based on a kinematic model of the hand. *IEEE Transactions on Instrumentation and Measurement*, 70:1–13, 2021.

[14] J. Shi, Y. Dai, Y. Cheng, S. Xie, G. Li, Y. Liu, J. Wang, R. Zhang, N. Bai, M. Cai, Y. Zhang, Y. Zhan, Z. Zhang, C. Yu, and C. Guo. Embedment of sensing elements for robust, highly sensitive, and cross-talk-free iontronic skins for robotics applications. *ScienceAdvances*, 9(9), 2023.

[15] C. J. Nycz, T. Bützer, O. Lambercy, J. Arata, S. F. Gregory, and R. Gassert. Design and characterization of a lightweight and fully portable remote actuation system for use with a hand exoskeleton. *IEEE Robotics and Automation Letters*, 1(2):976–983, 2016.

[16] D. Marconi, A. Baldoni, Z. McKinney, M. Cempini, S. Crea, and N. Vitiello. A novel hand exoskeleton with series elastic actuation for modulated torque transfer. *Mechatronics*, 61:69–82, 2019.

[17] A. Brygo, I. Sarakoglou, A. Ajoudani, N.G. Hernandez, G. Grioli, M. Catalano, D.G. Caldwell, and N. Tsagarakis. Synergy-based interface for bilateral tele-manipulations of a master-slave system with large asymmetries. In *2016 IEEE International Conference on Robotics and Automation (ICRA)*, pages 4859–4865, 2016.

[18] I. Sarakoglou, A. Brygo, D. Mazzanti, N.G. Hernandez, D.G. Caldwell, and N.G. Tsagarakis. , HEXOTRAC: A highly under-actuated hand exoskeleton for finger tracking and force feedback. In *2016 IEEE/RSJ International Conference on Intelligent Robots and Systems (IROS),Daejeon*, pages 1033–1040, 2016.

[19] F. C. Chen, S. Appendino, A. Battezzato, A. Favetto, M. Mousavi, and F. Pescarmona. Constraint Study for a Hand Exoskeleton: Human Hand Kinematics and Dynamics. *Journal of Robotics*, 2013, 2013.

[20] J. Lenarčič and T. Bajd and M.M. Stanišić. *RobotMechanisms*. Springer, 2013.